ACS APPLIED MATERIALS & INTERFACES

Research Article

Cite This: ACS Appl. Mater. Interfaces XXXX, XXX, XXX−XXX

www.acsami.org

Biomimetic Mineralization-Based CRISPR/Cas9 Ribonucleoprotein Nanoparticles for Gene Editing

Shuojun Li,[†,||] Zhiyong Song,[‡,||] Caiyun Liu,[§] Xiao-Lin Chen,*[,§] and Heyou Han*[,†,‡]

[†]State Key Laboratory of Agriculture Microbiology, College of Life Science and Technology, [‡]State Key Laboratory of Agriculture Microbiology, College of Science, and [§]The Provincial Key Laboratory of Plant Pathology of Hubei Province, College of Plant Science and Technology, Huazhong Agricultural University, Wuhan 430070, China

S Supporting Information

ABSTRACT: Delivery of the CRISPR/Cas9 ribonucleoprotein (RNP) complex has provided an alternative strategy for the regulation of CRISPR functions, offering a transient and DNA-free means for genomic editing. Chemical methods of delivering the RNPs via nanocomplexes have the potential to address these delivery problems for efficiency, safety, and packaging capacity. Here, we developed a biomimetic mineralization-mediated strategy for efficient DNA-free genome editing by using CRISPR/Cas9 RNPs. We found that the RNPs have the ability to form the biomimetic mineralized RNP nanoparticles (Bm-RNP NPs) quickly in situ and can be effectively delivered into the fungal protoplast cells. Biomimetic mineralization can maintain the natural function of Cas9 protein and protect the sgRNA activity. At the same time, the encapsulated RNPs can be effectively released into the cytoplasm, and the Sytalone dehydratase (SDH) gene can be edited in a targeted manner. Except for phenotypic defects, molecular detections indicated that the delivery of Bm-RNP NPs achieved 20% genomic editing for *Magnaporthe oryzae* compared to RNPs alone. Moreover, the Bm-RNP NP-mediated editing of the SDH gene significantly affects the appressorium-mediated penetration and invasive growth in *M. oryzae*. Our system has the advantages of being cheap, fast, and effective, without the traditional transformation process, suggesting the potential application of this DNA-free gene-editing strategy in different organisms.

KEYWORDS: CRISPR/Cas9 RNPs, gene editing, biomimetic mineralization, DNA-free, filamentous fungus
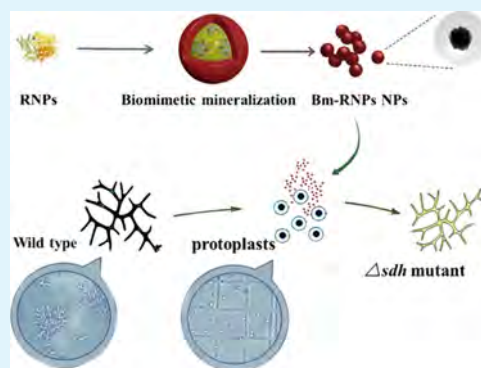
INTRODUCTION

The clustered regularly interspaced short palindromic repeat (CRISPR)-associated RNA-guided endonuclease (Cas9) technology has been widely used as a gene-editing tool because of its high efficiency and straightforward design.[1−4] Normally, the CRISPR/Cas9 system relies on the transfection of DNA encoding Cas9 and engineering sgRNA. During this process, there is a strong possibility of integration of the CRISPR/Cas9 DNA into the unknown genomic sites, which could increase off-target effects and produce unexpected genetic changes[5−7].

In order to avoid transgene integration, minimize off-target effects, and simplify the process, great efforts are being devoted to optimize the CRISPR/Cas9-mediated genome editing system and increase its application scope. Recently, delivery of the Cas9-sgRNA ribonucleoprotein (RNP) complex has provided an alternative strategy for the regulation of CRISPR functions, offering a transient and DNA-free means for genomic editing that could avoid transgene integration and greatly decrease off-target effects.[8] Despite a few reports about RNP delivery in bacteria[9] and plants,[10−16] there are rare reports of RNP delivery in filamentous fungi by current transformation methods,[17,18] and the CRISPR/Cas9 system still mainly relies on the insertion of the Cas9 gene so

far.[19−21] To address this problem, a number of RNPs delivery platforms have been developed in mammalian cells, such as the use of cell penetrating peptides, cationic lipid, gold nanoparticles, zeolitic imidazole frameworks, endosomal lysis agents, and receptor-mediated and endosomal escape agents such as PEI, to facilitate protein delivery into the cytosol.[22,23] Nevertheless, the RNP loading, releasing efficiency, simplicity, and stability of many methods are still limited,[24,25] particularly for large-sized proteins which have poor cell membrane permeability and sgRNA having high susceptibility to degradation and denaturation.[26,27] In nature, living organisms can produce various organic−inorganic nanocomposites, which exhibit optimal biocompatibility and biofriendlines.[28,29] Herein, we developed a nanovehicle for biomacromolecules based on quick biomimetic mineralization by calcium phosphate (CaP) under physiological conditions. We previously demonstrated that the CaP could encapsulate the antibody immunoglobulin molecule and control its release based on the physiological conditions and achieve the intracellular
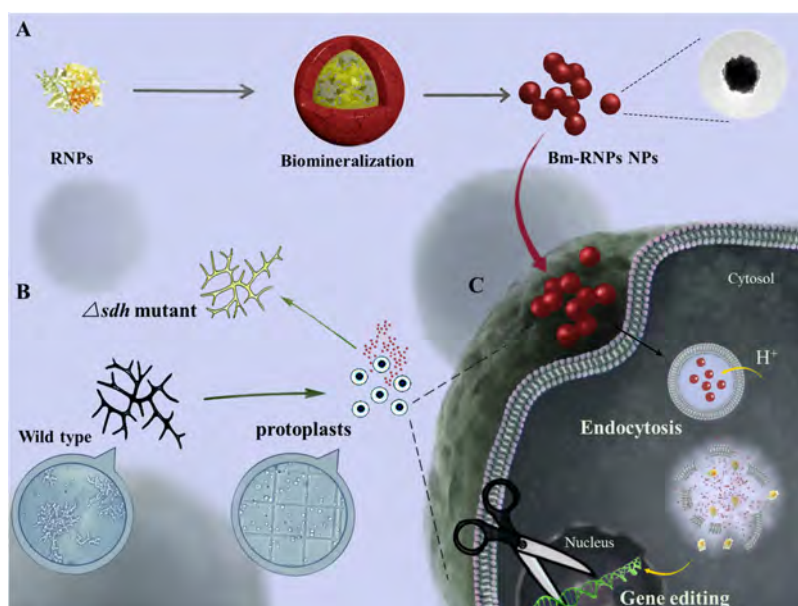
Figure 1. Overview of Bm-RNP NP-mediated genome editing in *M. oryzae*. (A) Fabrication of Bm-RNP NPs. (B) *M. oryzae* protoplasts were isolated and transformed. (C) RNPs were transferred into the nucleus through endocytosis.

antiviral effect, with the native structure and function of mAbs remaining unchanged after the biomimetic mineralization treatment.[30]

In this study, we report a novel strategy for CRISPR/Cas9 RNP delivery into a model plant pathogenic fungus, *Magnaporthe oryzae*, based on a biomimetic mineralization-mediated delivery system (Figure 1). We demonstrate that CRISPR/Cas9 RNPs can be efficiently mineralized to form RNP nanoparticles and delivered into intracellular protoplast cells, and mineralization treatment can maintain and protect the natural biological functions of the loaded biomacromolecules. The delivery of Bm-RNP NPs results in the successful knockout of the *M. oryzae* scytalone dehydratase (SDH) gene, leading to melanin deficiency. Furthermore, the phenotypic defects of Δ*sdh* mutants were analyzed through this gene-editing pathway. Calcium phosphate, as a pH responsive and bioavailability material, has been used for gene transfection and biomineralization widely. To our knowledge, this is the first report demonstrating a DNA-free genome editing method in a filamentous fungus using RNPs delivered by CaP biomimetic mineralization.

■ RESULTS

RNP Design and in Vitro Cleavage Assay. The purified recombinant Cas9 protein was obtained via the *Escherichia coli* expression system and purified by Ni-NTA (Figure S2), and sgRNAs were synthesized through in vitro transcription. The electrophoretograms indicated the basic components of the recombinant Cas9 protein (Figure S2), and the purified sgRNA product (Figure 2B) had a high purity. The sgRNA was designed for targeting the *SDH* gene in *M. oryzae*, and successful deletion would result in the white phenotype (Figure 2A).[31] The activity of Cas9-RNPs for gene editing was examined by in vitro cleavage assay of the function of RNPs. In our study, the 811 bp long polymerase chain reaction (PCR)-amplified product containing the *SDH* target region was used as the target DNA (Figure 2C line 1), and the results showed that the target sequence results in 491 and 320 bp long
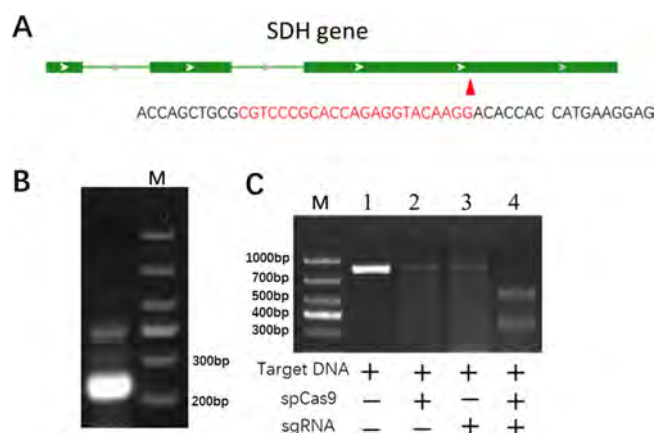

Figure 2. Preparation of RNPs. (A) Design of sgRNA targeting the *SDH* gene. (B) Gel electrophoresis of the sgRNA by in vitro transcription. (C) Cleavage assay to examine the functions of RNPs (line 4); lines 2 and 3 showed the addition of either sgRNA or Cas9 alone in the system.

products, which confirmed that the Cas9-RNPs have good activity.

We mixed the Cas9 and sgRNA at the molar ratio 1:1 to form Cas9-RNPs, followed by co-incubation with the target DNA, cleavage reaction for 50 min, and then agarose gel electrophoresis (AGE) assay. Densitometric analysis of the agarose gel indicated that the sgRNA-targeting *SDH* gene-directed Cas9-mediated cleavage achieved nearly 100% efficiency, and the two clear fragments indicated that RNPs had highly efficient and precise cleavage ability for the target dsDNA (Figure 2C line 4). In contrast, Cas9 or sgRNA alone was unable to influence the target DNA (Figure 2C line 2, 3). These results indicated the high cleavage efficiency of the RNPs targeting the *SDH* gene.

Fabrication of Bm-RNP NPs Based on Biomimetic Mineralization. After the formation of Cas9-RNPs from Cas9 and sgRNA, we fabricated Bm-RNP NPs and improved their dispersity using PAA (polyacrylic acid). Transmission electron
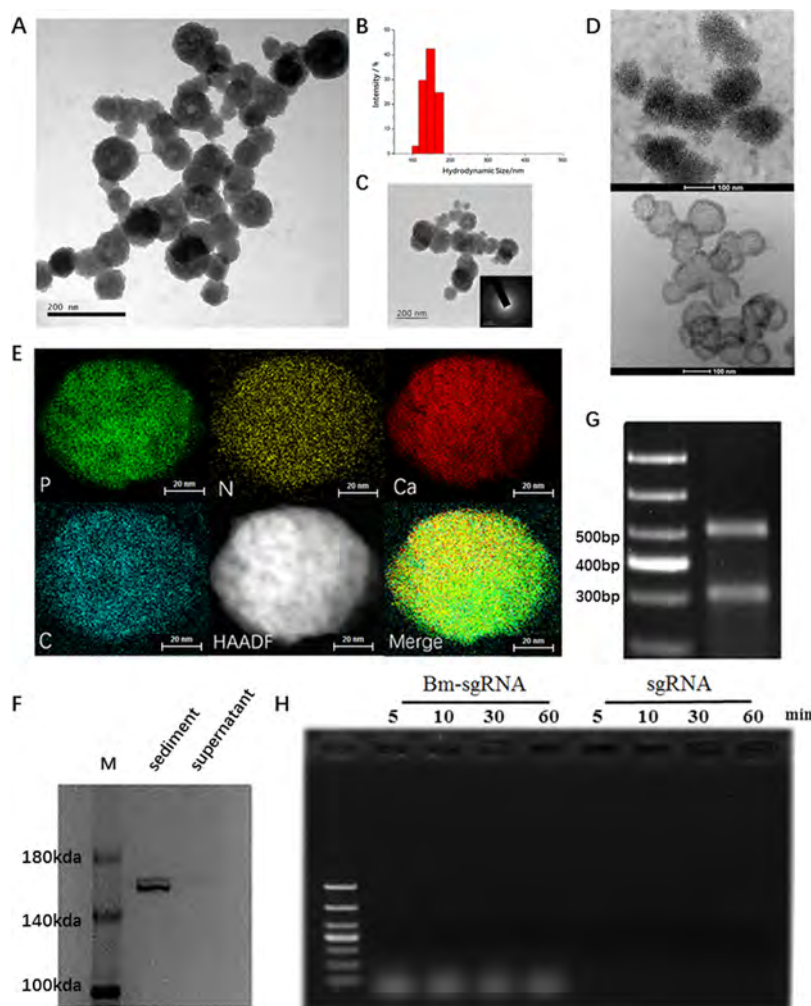
Figure 3. Characterization of Bm-RNP NPs. (A) TEM image of Bm-RNP NPs. (B) Size distribution of Bm-RNP NPs. (C) The selected area electron diffraction of Bm-RNP NPs. (D) Cryo-TEM image of the Bm-RNP NPs (left) and the pure CaP NPs (right). (E) Energy-dispersive X-ray spectrometry analysis of the Bm-RNP NPs. (F) Protein loading efficiency as detected by SDS-PAGE. (G) Activity of the Cas9 protein after release from Bm NPs. (H) Stability of Bm-sgRNA and sgRNA alone co-incubated with RNase. The sgRNA concentration was 50 ng/μL.

microscopy (TEM) (Figure 3A) and dynamic light scattering (DLS) analyses (Figure 3B) indicated that the Bm-RNP NPs had an average size of 100−200 nm and an ideal dispersity for intracellular delivery.[32,33] The selected area electron diffraction in TEM indicated that the CaP component was amorphous calcium phosphate (Figures 3C and S3). Using the high-resolution cryogenic TEM (cryo-TEM) and TEM, we found that the pure calcium phosphate nanoparticles were mostly hollow sphere-like but the Bm-RNP NPs were solid spheres (Figures 3D and S4). The sample composition was analyzed by energy-dispersive spectrometry (EDS) mapping. The image displayed the uniform distribution of Ca, P, C, N, and S elements in the same particle. These results confirmed the uniform deposition of protein and that nucleic acids were effectively loaded into biomimetic mineralized nanoparticles (Figures 3E and S5).

The loading efficiency of biomacromolecules in the process of biomimetic mineralization was evaluated by electrophoresis analysis using the Cas9 protein and pKNRG plasmid as the model. Our results showed that only a small amount of protein or DNA (2−5%) remained in the supernatant after biomimetic mineralization reaction (Figures 3F and S12a), indicating that most biomacromolecules were loaded to form biomimetic

mineralization nanoparticles (Bm NPs), and the loading efficiency reached nearly 100%. The effect of the mineralization process on the Cas9 function was investigated by releasing the Cas9 protein from the Bm NPs in the acidic conditions (pH 6−6.5) (Figure S6). The in vitro cleavage assay showed that the Cas9 protein still retained a high cleavage activity throughout the mineralization process (Figure 3G). To investigate whether the biomimetic mineralization treatment was able to protect sgRNA from enzymatic hydrolysis, the biomineralizaed sgRNA (Bm-sgRNA) and the pure sgRNA were co-incubated with Rnase (Figure 3F). The results showed that sgRNA alone were degraded immediately compared to the biomineralizaed sgRNA, which indicated that the biomimetic mineralization process can effectively improve the stability of RNA and thus improve the efficiency of gene editing in vivo. In order to evaluate the effect of the Cap concentration on enzyme activity, the sgRNA was co-incubated with Rnase in the slightly acidic biomimetic mineralization solution (bio-mimetic mineralization progress was not happening under pH = 6.0), and the results showed that the concentration of CaP did not inhibit the enzyme activity, even at a higher concentration (Figure S7). Furthermore, the effect of biomimetic mineralization treatment on DNA stability was
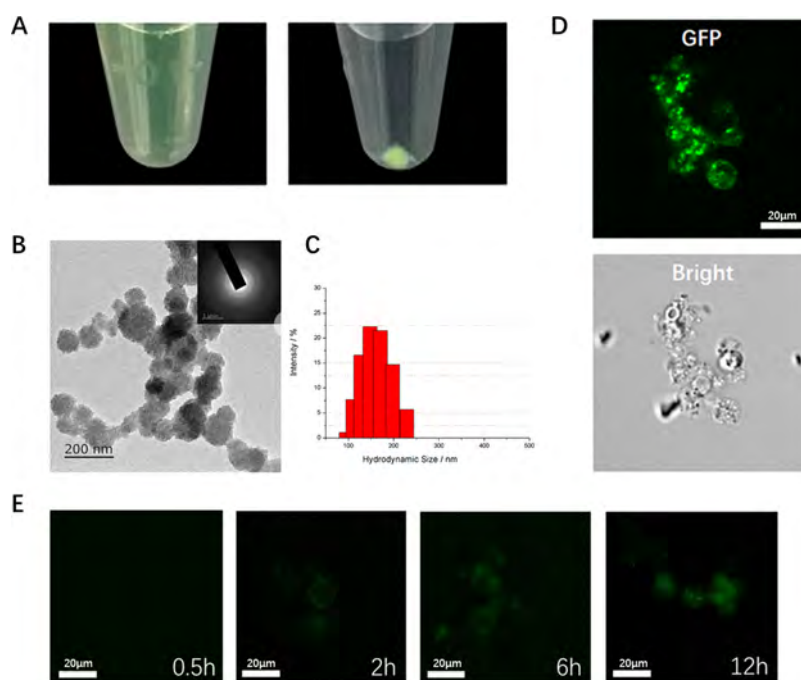
Figure 4. Delivery of the EGFP protein into *M. oryzae* protoplasts by Bm-EGFP NPs. (A) Image of Bm-EGFP NPs after centrifugation. (B) TEM image of the Bm-EGFP NPs. (C) Size distribution of Bm-EGFP NPs. (D) CLSM images of *M. oryzae* protoplasts after incubation with Bm-EGFP NPs. (E) The fluorescence images of the process for the Bm-EGFP NP delivery into the protoplast with the extension of time.

evaluated by co-incubation of DNA with DNase. The results showed that the biomineralized DNA still retained high stability, even after co-incubation with DNase for 12 h, while the pure DNA was degraded after 10 min DNase treatment (Figure S8). In the light of the above results, we can see that biomimetic mineralization treatment has the ability to protect biomacromolecules from enzymatic hydrolysis. Furthermore, to evaluate whether the biomimetic mineralization treatment affects protoplast regeneration, we observed the *M. oryzae* protoplast regeneration process while co-incubated with the Bm-RNP NPs. The microscopy result showed that the Bm-RNP NPs did not induce significant effects for protoplast regeneration, which revealed that the mineralization materials have good biocompatibility (Figure S9).

Evaluation of Biomimetic Mineralization Delivery Efficiency. To intuitively examine the intracellular delivery of the biomimetic mineralization, the recombinant EGFP protein was prepared as cargo to trace the process. After cloning the EGFP gene into pET-28a plasmid, the recombinant EGFP protein was obtained by prokaryotic expression and then purified by Ni-NTA. After purification, the protein showed an intense fluorescence (Figure S10). The Bm-EGFP NPs were concentrated by centrifugation after biomimetic mineralization, and the green deposit indicated that the EGFP protein was effectively loaded in the nanoparticles (Figure 4A). TEM and DLS size measurements indicated that biomimetic mineralized EGFP nanoparticles (Bm-EGFP NPs) had a similar morphology and size distribution to that of Bm-RNP NPs (Figure 4B,C), indicating that it can directly reflect the intracellular protein delivery process by biomimetic mineralization treatment. After the recombinant EGFP protein was mineralized and co-incubated with the protoplasts for 24 h, the confocal laser scanning microscopy (CLSM) result showed that the cell was surrounded by green fluorescence and part of the fluorescence was dispersed in the cytoplasm (Figure 4D),

revealing that Bm-EGFP NPs were attached to the surface of the cell membrane. This may increase the chance of cell uptake through the endocytosis pathway. The endosomal escape of Bm NPs is mediated by the buffering capacity of the calcium phosphate, which is followed by the release of cargo to the cytoplasm.[34] Moreover, a fluorescence microscope was used to track the EGFP protein delivery process, and the fluorescence intensity in the *M. oryzae* cell was observed to increase gradually with the extension of time (Figure 4E), exhibiting the high protein delivery ability-based biomimetic mineralization. To investigate whether the biomimetic mineralized strategy has a general applicability in other species, we deliver an EGFP fusion nuclear localization sequence into the HeLa cell by the biomimetic mineralized GFP nanoparticles. CLSM images showed that the delivered GFP dispersed and reached into the nucleus efficiently (Figure S11).

Furthermore, pKNRG was prepared as the GFP expression vector for the transient transfection of *M. oryzae*.[35] After the plasmid vector was subjected to biomimetic mineralization treatment to form biomimetic mineralized plasmid nanoparticles (Bm-plasmid NPs) and transfected into protoplasts, DLS analysis indicated that the Bm-plasmid NPs had a similar size distribution to that of Bm-RNP NPs. After 24 h transfection, the GFP expression was validated by CLSM. Fluorescence analysis revealed the GFP expression in protoplast cells (Figure S12), which further demonstrated the good application of the biomineralization strategy in biomacromolecule delivery.

Gene Editing in *M. oryzae* by Biomimetic Mineralized Nanoparticles. After confirming the high efficiency of the biomimetic mineralization strategy in delivering protein and nucleic acids into the protoplasts, we attempted to deliver Cas9-RNPs for gene editing. The assembled Bm-RNP NPs targeting the *SDH* gene were added into the protoplasts and co-incubated overnight. After cell wall regeneration, we coated
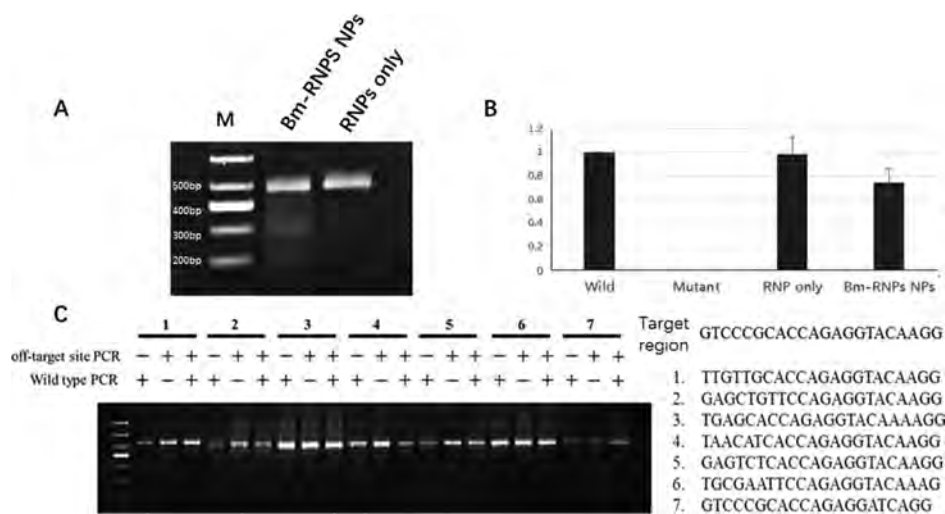
Figure 5. Genome editing of *M. oryzae* by Bm-RNP NPs. (A) T7E1 assay for the indel frequency analysis. (B) Quantitation of the *SDH* gene expression by qRT-PCR. (C) T7E1 analysis of the potential off-target effect in *M. oryzae* induced by Bm-RNP NPs.
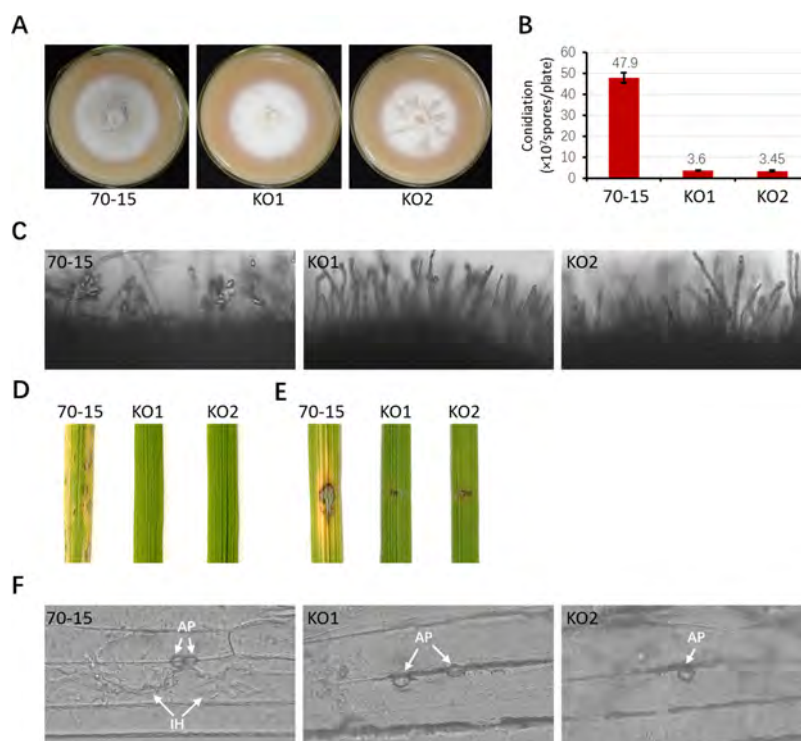
Figure 6. Functional determination of the knockout mutants of *SDH*. (A) Phenotype of the colony. (B) Amount of conidia. (C) Microscopic image of the conidiophores. (D,E) Pathogenicity of the conida and mycelial on the rice seedlings. (F) Image of the appressoria form. AP, appressorium; IH, infection hyphae.

the diluted protoplasts on CM plates to select the Δ*sdh* mutant, and the white mutant could be easily identified at the early mycelium growth stage (after 3 days of incubation) (Figure S13).

The effect of Bm-RNP NPs on gene editing was also evaluated. The DSBs derived from RNP-targeted DNA would drive the formation of indels (insertion or deletion) by the NHEJ repair pathway, and the T7 endonuclease-I assay was used to detect the indel percentage because of the reason that re-annealed heteroduplexes can be cleaved by T7E1.[36] After co-incubation with Bm-RNP NPs and cell wall regeneration, the protoplasts were collected to extract the mixed genomic

DNA, from which the mixed *SDH* gene fragment was amplified and then re-annealed slowly to generate heteroduplexes.

Additionally, we replaced the primers to eliminate the mispairing interference from the polyA structure in the *SDH* gene region. The T7E1 assay indicated that the gene edit efficiency was up to 20% through the mineralization process (Figure 5A). The sequence analysis revealed that most indels resulted from the insertion of thymine in the targeted locus (we analyzed five monoclones with Δ*sdh* mutations) (Figure S14). Meanwhile, quantitative real-time PCR (qRT-PCR) was performed to quantify the mRNA levels of the *SDH* gene. The results exhibited that the Δ*sdh* had no *SDH* gene expression,

E

and the *SDH* gene expression decreased notably in the Bm-RNP NP-treated protoplasts. In contrast, the treatment of RNPs alone had no obvious effect on the *SDH* gene expression (Figure 5B).

To evaluate potential off-target effects of the Bm-RNP NPs, we used the online Basic Local Alignment Search Tool to find seven potential sites matching the on-target sequence with similarity and most likely to induce off-target effects. T7E1 analysis indicated that *M. oryzae* treated with Bm-RNP NPs showed no significant cleavage in the seven potential off-targeted sites (Figure 5C).

Functional Determination of the CRISPR Disruption Mutants of *SDH*. To investigate whether the function of *SDH* is affected by the editing, we observed the phenotypic defects of the CRISPR-edited mutants. The Δ*sdh* was normal in colony size, but was evidently much whiter than the wild type (Figure 6A), indicating that *SDH* is required for the fungal mycelial pigmentation, which is consistent with its predicted function in melanin biosynthesis. Conidiation of the Δ*sdh* mutant was also significantly reduced (Figure 6B). The microscopic observation demonstrated that the Δ*sdh* mutant formed sparse conidia on the conidiophores, while the wild type formed the dense cluster of conidiophores (Figure 6C). These results indicated that the CRISPR editing of *SDH* affects the conidiation and conidiophore formation in the rice blast fungus. Importantly, disruption of *SDH* led to loss of pathogenicity (Figure 6D). Even when inoculated onto the wounded rice leaves, the Δ*sdh* mutant still cannot form disease symptoms (Figure 6E), indicating that disruption of *SDH* affects host colonization. By observing the host cell, we found that the penetration and invasive growth of the Δ*sdh* mutant in the host cell was significantly blocked (Figure 6F). These results indicated that the CRISPR-mediated editing of *SDH* significantly affects the appressorium-mediated penetration and invasive growth in *M. oryzae*.

■ DISCUSSION

Direct and efficient delivery of CRISPR/Cas9-RNPs into the cytosol that avoids transgene integration and reduces off-target effects remains a challenge.[22,37] In this work, we designed a biomimetic mineralization-mediated strategy for efficient DNA-free genome editing on eukaryotic cells based on the delivery of RNPs. Considering convenience and overwhelming importance, we used the rice blast fungus *M. oryzae* as a model eukaryotic organism to test our biomimetic mineralized nanoparticle-based delivery of CRISPR/Cas9 RNP for DNA-free gene editing. As a consequence, we successively developed an efficient and novel CRISPR/Cas9 genome editing method to promote genetic improvement for this fungus. Obviously, this strategy could be conveniently expanded into different eukaryotic organisms.

Usually, it is difficult to achieve an efficient and direct delivery of the native protein biomacromolecule into the cytosol owing to endosomal entrapment and systemic toxicity, but CaP NPs, pH responsive and bioavailable materials, are able to efficiently load and release proteins in an intracellular environment.[38] In nature, biomimetic mineralization is regarded as an effective tactic for living organisms to become biologically "stealthy" and protect themselves from external damage by producing a wide range of organic−inorganic hybrid materials.[29] Inspired by biomimetic mineralization, we have developed Bm-RNP NPs in situ, which were characterized by TEM as solid sphere-like, which have good

dispersion and uniform size and can achieve more effective intracellular delivery with a diameter of 100−200 nm (Figure 3). However, the pure calcium phosphate nanoparticles were mostly hollow spheres as previously described.[39] Previous reports have shown that CaP NPs have been widely used as nanovectors for intracellular delivery,[40,41] and intermediate sizes (20−200 nm) have the highest potential for in vivo applications.[42] Furthermore, the in vitro release analysis demonstrated that the Bm-RNP NPs were stable under physiological conditions and could be quickly dissolved (within several seconds) in the acidic solution (pH < 6.5). A previous report has shown that most of the calcium phosphate biomimetic mineralization process took at least 2 h.[30,43,44] However, our mineralization reaction time was significantly reduced, and the whole loading process only took 3−5 min, which can avoid the degradation of biomacromolecules during the assembly process. These unique biological properties also implied that the biomimetic mineralization treatment did not alter the native structure and the function of Cas9, but can effectively protect the nucleic acids and proteins from enzymatic degradation and deliver them into cells. Previous studies have shown that after entering the cells, the Cap nanoformulations would de-assemble at low pH in the endosome (pH = 4.0−5.0), which would cause endosome swelling and bursting to release the entrapped cargo.[45] Our results show that, in addition to RNP complexes, other biological macromolecules could also effectively prepare nanoparticles through biomimetic mineralization to achieve effective intracellular delivery, such as plasmid and EGFP protein. In contrast to other techniques, the in situ biomimetic mineralization-based modification of RNPs is feasible, universal, biocompatible, and inexpensive. The abovementioned experimental results show that biomimetic mineralization can be developed as a technique to overcome the hurdles imposed by the intracellular delivery of RNPs.

The DNA-free genome modification has been demonstrated in precision crop breeding, but compared to the numerous delivery methods in animal systems, these studies on RNP delivery in plants mainly rely on biolistics. For both of the multicellular fungus and plants, transformation methods are the primary strategy through the DNA insert to achieve genomic editing such as *Agrobacterium*-mediated fungal transformation.[46,47] RNP delivery can avoid the continuous expression of the CRISPR/Cas9 DNA, without the necessity to select a suitable plasmid driving Cas9 and sgRNAs according to different species. Other than fungi or plants, this universal and transient gene-editing strategy may have potential application in different organisms in the future. Furthermore, we used the in vitro cleavage assay to confirm the efficiency of the RNP activity prior to intracellular gene editing. An excellent in vitro targeting ability is essential for in vivo gene editing. In previous reports, the incidence of HDR might be higher in filamentous fungi than that in animals or plants because of the ectopic HDR, although NHEJ repair is the main pathway in many eukaryotic cells.[48] HDR is considered as a precise DNA repair pathway, implicating that the CRISPR/Cas9-resulting DSB-mediated gene knockout based on NHEJ repair may encounter some obstacles in filamentous fungi. However, in our experiment, except for phenotypic defects, the gene knockout efficiency was increased at least by 20% in *M. oryzae* when compared to the RNPs alone. This might result from the uptake of abundant RNPs by protoplasts through this Bm-RNP NP delivery pathway, leading to a notable effect on

the genomic DNA and the production of a mass of DSBs. Therefore, the genome editing using biomimetic mineralized CRISPR/Cas9 RNPs may provide a universal and DNA-free method for improving editing efficiency.

■ CONCLUSIONS

In summary, we established an efficient and specific biomimetic mineralized CRISPR/Cas9 RNP NP-mediated genome editing method. Our study suggests that the strategy will greatly facilitate the specific and clean genome editing in a wide range of eukaryotic organisms.

■ EXPERIMENTAL SECTION

Expression and Purification of spCas9 Protein. The spCas9 gene was cloned into pET-28b (addgene id = 47327) and transformed in *E. coli* BL21 (DE3) strain (Figure S1). The single clone was transferred into 10 mL of LB (kana) media from the selective plate at 37 °C and 220 rpm overnight and then inoculated into 1 L of LB media for protein expression, followed by induction with 0.75 mM isopropyl β-D-1-thiogalactopyranoside (IPTG) at 16 °C for 15 h. Next, the cells were harvested by centrifugation (7500 rpm, 40 min) and resuspended in lysis buffer (150 mM NaCl, 10 mM Tris-HCl, 0.05% β-mercaptoethanol, and pH = 7.5). For extracting the Cas9 protein, cells were lysed by sonication on ice, and then, the supernatant was collected for purification by Ni-NTA affinity chromatography using buffer B (250 mM imidazole, 300 mM NaCl, and pH = 7.5) to wash Cas9 protein. The eluant was ultrafiltrated to replace the storage buffer (50 mM Tris-HCl, 300 mM NaCl, 0.1 mM ethylenediaminetetraacetic acid, 20% glycerol, 1 mM dithiothreitol, 0.5 mM phenylmethylsulfonyl fluoride, and pH = 8.0) with the buffer renewed every 20 min. The purity of the final purified product was determined using sodium dodecyl sulfate-polyacrylamide gel electrophoresis (SDS-PAGE) (6%).

Design and Synthesis of sgRNA. sgRNA was synthesized by T7 in vitro transcription from the double-stranded DNA template (contains target sequence, trace RNA and T7 promoter) using an RNA in vitro transcription kit (Takara, Japan). To target the SDH gene, the forward primer sequence was designed as CCTCTAA-TACGACTCACTATAGG<u>CGTCCCGCACCAGA GGTACA</u>GTT-TAAGAGCTATGC (target sequence is underlined). The sgRNA was purified using the RNA purification kit (Takara, Japan) and examined by AGE.

RNP Activity in Vitro Assay. The PCR primers SCR-F and SCR-R (Table S1) were used to amplify the target DNA from *M. oryzae* genomic DNA extracted from the plant DNA extraction kit (Takara, Japan) using the mycelium according to the user manual. The PCR products were purified by DNA gel extraction. The Cas9 protein (1 μg) and sgRNA were mixed at the molar ratio 1:1 at 37 °C for 5 min to form Cas9-RNPs, which were added into target DNA (250 ng) and incubated at 37 °C for 50 min for cleavage reaction and the subsequent AGE assay.

RNP Biomimetic Mineralization and Characterization. Cas9 and sgRNA were mixed at the molar ratio 1:1 at 37 °C for 10 min to form Cas9-RNPs. Next, 50 μL of RNPs (50 μg) was mixed with 183 μL of buffer A (20 mM Tris-HCl, 300 mM NaCl, pH = 7.5) and vortexed, followed by the addition of 10.4 μL of 60 mM Na_2HPO_4 and vortexing and then the addition of 25 μL of 100 mM $CaCl_2$ and vortexing. After standing at room temperature for 5 min, the clear solution turned opaque quickly, followed by the addition of 5 μL of 1 M PAA and vortexing to improve the NP dispersion. After three washes in ddH_2O, the Bm-RNP NPs were separated by centrifugation at 10 000 rpm for 10 min and then resuspended with ddH2O and ultrasonic dispersion. The nanoparticles were characterized by tunneling electron microscopy (Hitachi, Japan), high-resolution cryogenic TEM (FEI, USA), and EDS-mapping. The size and polydispersity index of the Bm-RNP NPs were measured using DLS (Malvern, England).

Analysis of Biomimetic Mineralization Efficiency and Protection Assay. The protein and DNA biomimetic mineralization efficiency was examined by SDS-PAGE and AGE. Specifically, 25 μL of Cas9 (1 μg/μL) and 25 μL of pKNRG plasmid (340 ng/μL) were biomimetic mineralized separately as described above, and the control group was prepared in the same method, but with $CaCl_2$ replaced by buffer A, followed by electrophoretic analysis of the supernatant from each group. For the description above, Cas9 protein was biomimetic mineralized and then collected by centrifugation. After resuspending the Bm NP precipitation in storage buffer, 0.1 M HCl was used to dissolve the Bm NPs. Soon, the opaque solution turned clear, and the resulting Cas9 was used for the in vitro assay. The effect of Bm NPs on sgRNA or DNA stability was evaluated by using sgRNA or PCR products as cargo, followed by the addition of the 3 μL of RNaseA or recombinant DNase (Takara, Japan) to the reaction system and incubation at 37 °C for different periods of time, with unbiomimetic mineralized PCR products used as the control. 10× loading buffer was used to terminate hydrolysis reaction and for electrophoretic analysis.

M. oryzae Protoplast Preparation. *M. oryzae* mycelia were inoculated into the liquid CM culture (0.6% yeast extract, 0.3% enzymatic casein hydrolysate, 0.3% acidic casein hydrolysate, and 1% D-glucose) and grown at 28 °C for 36 h. Then, the mycelia were transferred into 9 mL of 0.7 M NaCl for enzymolysis, followed by the addition of 0.1 M Lyticase (Lysing Enzymes from *Trichoderma harzianum*, Sigma) and incubation at 30 °C and 180 rpm for 3 h. The protoplasts were obtained by using lens paper and then resuspended in the LR liquid culture (34.2% sucrose, 1% enzymatic casein hydrolysate, 1% yeast extract) after three washes in 0.7 M NaCl.

Intracellular Delivery Efficiency by GFP. The EGFP gene was cloned into the pET-28a vector using primers EGFP-F and EGFP-R (Table S1) from pEGFP-C1 plasmid. The recombinant vector was transformed into *E. coli* BL21 (DE3) strain for expression and purified by Ni-NTA. The EGFP expression plasmid for *M. oryzae* was constructed from the pKNRG plasmid (Figure S6). The recombinant EGFP protein was biomimetic mineralized as described above. The Bm-EGFP NPs were dispersed in 50 μL of the LR liquid culture and then supplemented with 200 μL of 10^7 protoplasts, followed by co-incubation at 28 °C for 24 h and then determining the intracellular delivery efficiency by confocal microscopy (Leica, German) and fluorescence microscopy (Echo, USA).

Gene Editing by Bm-RNP NPs. The Bm-RNP NPs fabricated as described above and the assembled Bm-RNP NPs targeting the SDH gene were added into the protoplasts and incubated in the LR liquid culture overnight. After cell wall regeneration, the cells were diluted by coating them separately on CM plates at 28 °C for mycelial growth. In the coated plates, the compact mycelia were grown and the single clone with the white phenotype was inoculated into new plates for phenotypic characterization and sequencing, or the protoplasts were directly used to extract the mix genomic DNA for indel analysis after co-incubation with Bm-RNP NPs. The PCR products amplified with primers SDH-F and SDH-F (Table S1) were used to evaluate the genome editing efficiency by T7E1 indel analysis (Neb, English). The total RNA extracted from protoplasts and primers actin-F, actin-R, RT-SDH-F, and RT-SDH-R (Table S1) was used for RT-PCR (analytikjena, German). Primers (Table S1) were used to analyze the potential off-target effect.

■ ASSOCIATED CONTENT

Ⓢ Supporting Information

The Supporting Information is available free of charge at https://pubs.acs.org/doi/10.1021/acsami.9b17598.

Supporting Information, Figures S1−S14, Table S1 (PDF)

■ AUTHOR INFORMATION

Corresponding Authors
*E-mail: chenxiaolin@mail.hzau.edu.cn (X.-L.C.).
*E-mail: hyhan@mail.hzau.edu.cn (H.H.).

ORCID ⊙

Zhiyong Song: 0000-0002-2552-5239
Heyou Han: 0000-0001-9406-0722

Author Contributions

∥S.L. and Z.S. contributed equally to this work.

Notes

The authors declare no competing financial interest.

■ REFERENCES

(1) Hsu, P. D.; Lander, E. S.; Zhang, F. Development and Applications of CRISPR-Cas9 for Genome Engineering. *Cell* **2014**, *157*, 1262−1278.

(2) Wang, H.; La Russa, M.; Qi, L. S. CRISPR/Cas9 in Genome Editing and Beyond. *Annu. Rev. Biochem.* **2016**, *85*, 227−264.

(3) Barrangou, R.; Doudna, J. A. Applications of CRISPR Technologies in Research and Beyond. *Nat. Biotechnol.* **2016**, *34*, 933−941.

(4) Wright, A. V.; Nuñez, J. K.; Doudna, J. A. Biology and Applications of CRISPR Systems: Harnessing Nature's Toolbox for Genome Engineering. *Cell* **2016**, *164*, 29−44.

(5) Kim, J.; Kim, J.-S. Bypassing GMO Regulations with CRISPR Gene Editing. *Nat. Biotechnol.* **2016**, *34*, 1014−1015.

(6) Yin, H.; Kanasty, R. L.; Eltoukhy, A. A.; Vegas, A. J.; Dorkin, J. R.; Anderson, D. G. Non-viral Vectors for Gene-based Therapy. *Nat. Rev. Genet.* **2014**, *15*, 541−555.

(7) Gorbunova, V.; Levy, A. A. Non-homologous DNA End Joining in Plant Cells is Associated with Deletions and Filler DNA Insertions. *Nucleic Acids Res.* **1997**, *25*, 4650−4657.

(8) Liang, X.; Potter, J.; Kumar, S.; Zou, Y.; Quintanilla, R.; Sridharan, M.; Carte, J.; Chen, W.; Roark, N.; Ranganathan, S.; Ravinder, N.; Chesnut, J. D. Rapid and Highly Efficient Mammalian Cell Engineering via Cas9 Protein Transfection. *J. Biotechnol.* **2015**, *208*, 44−53.

(9) Kang, Y. K.; Kwon, K.; Ryu, J. S.; Lee, H. N.; Park, C.; Chung, H. J. Nonviral Genome Editing Based on a Polymer-Derivatized CRISPR Nanocomplex for Targeting Bacterial Pathogens and Antibiotic Resistance. *Bioconjugate Chem.* **2017**, *28*, 957−967.

(10) Liang, Z.; Chen, K.; Zhang, Y.; Liu, J.; Yin, K.; Qiu, J.-L.; Gao, C. Genome Editing of Bread Wheat Using Biolistic Delivery of CRISPR/Cas9 in vitro Transcripts or Ribonucleoproteins. *Nat. Protoc.* **2018**, *13*, 413.

(11) Liang, Z.; Chen, K.; Li, T.; Zhang, Y.; Wang, Y.; Zhao, Q.; Liu, J.; Zhang, H.; Liu, C.; Ran, Y.; Gao, C. Efficient DNA-free Genome Editing of Bread Wheat Using CRISPR/Cas9 Ribonucleoprotein Complexes. *Nat. Commun.* **2017**, *8*, 14261.

(12) Malnoy, M.; Viola, R.; Jung, M. H.; Koo, O. J.; Kim, S.; Kim, J. S.; Velasco, R.; Nagamangala Kanchiswamy, C. DNA-Free Genetically Edited Grapevine and Apple Protoplast Using CRISPR/Cas9 Ribonucleoproteins. *Front. Plant Sci.* **2016**, *7*, 1904.

(13) Subburaj, S.; Chung, S. J.; Lee, C.; Ryu, S.-M.; Kim, D. H.; Kim, J.-S.; Bae, S.; Lee, G.-J. Site-directed Mutagenesis in Petunia x Hybrida Protoplast System Using Direct Delivery of Purified Recombinant Cas9 Ribonucleoproteins. *Plant Cell Rep.* **2016**, *35*, 1535−1544.

(14) Palocci, C.; Valletta, A.; Chronopoulou, L.; Donati, L.; Bramosanti, M.; Brasili, E.; Baldan, B.; Pasqua, G. Endocytic Pathways Involved in PLGA Nanoparticle Uptake by Grapevine Cells and Role of Cell Wall and Membrane in Size Selection. *Plant Cell Rep.* **2017**, *36*, 1917−1928.

(15) Liang, Z.; Chen, K.; Yan, Y.; Zhang, Y.; Gao, C. Genotyping Genome-edited Mutations in Plants Using CRISPR Ribonucleoprotein Complexes. *Plant Biotechnol. J.* **2018**, *16*, 2053.

(16) Andersson, M.; Turesson, H.; Olsson, N.; Falt, A.-S.; Ohlsson, P.; Gonzalez, M. N.; Samuelsson, M.; Hofvander, P. Genome Editing in Potato via CRISPR-Cas9 Ribonucleoprotein Delivery. *Physiol. Plant.* **2018**, *164*, 378.

(17) Wang, Q.; Cobine, P. A.; Coleman, J. J. Efficient Genome Editing in Fusarium Oxysporum Based on CRISPR/Cas9 Ribonucleoprotein Complexes. *Fungal Genet. Biol.* **2018**, *117*, 21−29.

(18) Foster, A. J.; Martin-Urdiroz, M.; Yan, X.; Wright, H. S.; Soanes, D. M.; Talbot, N. J. CRISPR-Cas9 Ribonucleoprotein-mediated Co-editing and Counterselection in the Rice Blast Fungus. *Sci. Rep.* **2018**, *8*, 14355.

(19) Nødvig, C. S.; Nielsen, J. B.; Kogle, M. E.; Mortensen, U. H. A CRISPR-Cas9 System for Genetic Engineering of Filamentous Fungi. *PLoS One* **2015**, *10*, No. e0133085.

(20) Wenderoth, M.; Pinecker, C.; Voss, B.; Fischer, R. Establishment of CRISPR/Cas9 in Alternaria Alternata. *Fungal Genet. Biol.* **2017**, *101*, 55−60.

(21) Arazoe, T.; Miyoshi, K.; Yamato, T.; Ogawa, T.; Ohsato, S.; Arie, T.; Kuwata, S. Tailor-made CRISPR/Cas System for Highly Efficient Targeted Gene Replacement in the Rice Blast Fungus. *Biotechnol. Bioeng.* **2015**, *112*, 2543−2549.

(22) Wang, H.-X.; Li, M.; Lee, C. M.; Chakraborty, S.; Kim, H.-W.; Bao, G.; Leong, K. W. CRISPR/Cas9-based Genome Editing for Disease Modeling and Therapy: Challenges and Opportunities for Nonviral Delivery. *Chem. Rev.* **2017**, *117*, 9874−9906.

(23) Wan, T.; Niu, D.; Wu, C.; Xu, F.-J.; Church, G.; Ping, Y. Material Solutions for Delivery of CRISPR/Cas-based Genome Editing Tools: Current Status and Future Outlook. *Mater. Today* **2019**, *26*, 40−66.

(24) Yue, H.; Zhou, X.; Cheng, M.; Xing, D. Graphene Oxide-mediated Cas9/sgRNA Delivery for Efficient Genome Editing. *Nanoscale* **2018**, *10*, 1063−1071.

(25) Chen, T.-T.; Yi, J.-T.; Zhao, Y.-Y.; Chu, X. Biomineralized Metal-Organic Framework Nanoparticles Enable Intracellular Delivery and Endo-Lysosomal Release of Native Active Proteins. *J. Am. Chem. Soc.* **2018**, *140*, 9912−9920.

(26) Pakulska, M. M.; Miersch, S.; Shoichet, M. S. Designer Protein Delivery: From Natural to Engineered Affinity-controlled Release Systems. *Science* **2016**, *351*, aac4750.

(27) D'Astolfo, D. S.; Pagliero, R. J.; Pras, A.; Karthaus, W. R.; Clevers, H.; Prasad, V.; Lebbink, R. J.; Rehmann, H.; Geijsen, N. Efficient Intracellular Delivery of Native Proteins. *Cell* **2015**, *161*, 674−690.

(28) Yao, S. S.; Jin, B. A.; Liu, Z. M.; Shao, C. Y.; Zhao, R. B.; Wang, X. Y.; Tang, R. K. Biomineralization: From Material Tactics to Biological Strategy. *Adv. Mater.* **2017**, *29*, 1605903.

(29) Dorozhkin, S. V.; Epple, M. Biological and Medical Significance of Calcium Phosphates. *Angew. Chem., Int. Ed.* **2002**, *41*, 3130−3146.

(30) Song, Z.; Liu, L.; Wang, X.; Deng, Y.; Nian, Q.; Wang, G.; Zhu, S.; Li, X.; Zhou, H.; Jiang, T.; Xu, X.; Tang, R.; Qin, C. Intracellular Delivery of Biomineralized Monoclonal Antibodies to Combat Viral Infection. *Chem. Commun.* **2016**, *52*, 1879−1882.

(31) Arazoe, T.; Ogawa, T.; Miyoshi, K.; Yamato, T.; Ohsato, S.; Sakuma, T.; Yamamoto, T.; Arie, T.; Kuwata, S. Tailor-made TALEN System for Highly Efficient Targeted Gene Replacement in the Rice Blast Fungus. *Biotechnol. Bioeng.* **2015**, *112*, 1335−1342.

(32) Alsaiari, S. K.; Patil, S.; Alyami, M.; Alamoudi, K. O.; Aleisa, F. A.; Merzaban, J. S.; Li, M.; Khashab, N. M. Endosomal Escape and Delivery of CRISPR/Cas9 Genome Editing Machinery Enabled by Nanoscale Zeolitic Imidazolate Framework. *J. Am. Chem. Soc.* **2018**, *140*, 143−146.

(33) Jiang, W.; Kim, B. Y. S.; Rutka, J. T.; Chan, W. C. W. Nanoparticle-mediated Cellular Response is Size-dependent. *Nat. Nanotechnol.* **2008**, *3*, 145−150.

(34) Kester, M.; Heakal, Y.; Fox, T.; Sharma, A.; Robertson, G. P.; Morgan, T. T.; Altinoğlu, E. I.; Tabaković, A.; Parette, M. R.; Rouse, S. M.; Ruiz-Velasco, V.; Adair, J. H. Calcium Phosphate Nanocomposite Particles for in vitro Imaging and Encapsulated Chemotherapeutic Drug Delivery to Cancer Cells. *Nano Lett.* **2008**, *8*, 4116−4121.

(35) Liu, C.; Li, Z.; Xing, J.; Yang, J.; Wang, Z.; Zhang, H.; Chen, D.; Peng, Y.-L.; Chen, X.-L. Global Analysis of Sumoylation Function Reveals Novel Insights into Development and Appressorium-mediated Infection of the Rice Blast Fungus. *New Phytol.* **2018**, *219*, 1031−1047.

(36) Ran, F. A.; Hsu, P. D.; Wright, J.; Agarwala, V.; Scott, D. A.; Zhang, F. Genome Engineering Using the CRISPR-Cas9 System. *Nat. Protoc.* **2013**, *8*, 2281−2308.

(37) Li, L.; He, Z.-Y.; Wei, X.-W.; Gao, G.-P.; Wei, Y.-Q. Challenges in CRISPR/Cas9 Delivery: Potential Roles of Nonviral Vectors. *Hum. Gene Ther.* **2015**, *26*, 452−462.

(38) Huang, X.; Andina, D.; Ge, J.; Labarre, A.; Leroux, J.-C.; Castagner, B. Characterization of Calcium Phosphate Nanoparticles Based on a PEGylated Chelator for Gene Delivery. *ACS Appl. Mater. Interfaces* **2017**, *9*, 10435−10445.

(39) Hagmeyer, D.; Ganesan, K.; Ruesing, J.; Schunk, D.; Mayer, C.; Dey, A.; Sommerdijk, N. A. J. M.; Epple, M. Self-assembly of Calcium Phosphate Nanoparticles into Hollow Spheres Induced by Dissolved Amino Acids. *J. Mater. Chem.* **2011**, *21*, 9219−9223.

(40) Morgan, T. T.; Muddana, H. S.; Altinoğlu, E. I.; Rouse, S. M.; Tabaković, A.; Tabouillot, T.; Russin, T. J.; Shanmugavelandy, S. S.; Butler, P. J.; Eklund, P. C.; Yun, J. K.; Kester, M.; Adair, J. H. Encapsulation of Organic Molecules in Calcium Phosphate Nanocomposite Particles for Intracellular Imaging and Drug Delivery. *Nano Lett.* **2008**, *8*, 4108−4115.

(41) Scaletti, F.; Hardie, J.; Lee, Y.-W.; Luther, D. C.; Ray, M.; Rotello, V. M. Protein Delivery into Cells Using Inorganic Nanoparticle-protein Supramolecular Assemblies. *Chem. Soc. Rev.* **2018**, *47*, 3421−3432.

(42) Canton, I.; Battaglia, G. Endocytosis at the Nanoscale. *Chem. Soc. Rev.* **2012**, *41*, 2718−2739.

(43) Wang, G.; Li, X.; Mo, L.; Song, Z.; Chen, W.; Deng, Y.; Zhao, H.; Qin, E.; Qin, C.; Tang, R. Eggshell-inspired Biomineralization Generates Vaccines that Do Not Require Refrigeration. *Angew. Chem., Int. Ed.* **2012**, *51*, 10576−10579.

(44) Wang, G.; Cao, R.-Y.; Chen, R.; Mo, L.; Han, J.-F.; Wang, X.; Xu, X.; Jiang, T.; Deng, Y.-Q.; Lyu, K.; Zhu, S.-Y.; Qin, E.-D.; Tang, R.; Qin, C.-F. Rational Design of Thermostable Vaccines by Engineered Peptide-induced Virus Self-biomineralization Under Physiological Conditions. *Proc. Natl. Acad. Sci. U.S.A.* **2013**, *110*, 7619−7624.

(45) Li, J.; Chen, Y.-C.; Tseng, Y.-C.; Mozumdar, S.; Huang, L. Biodegradable Calcium Phosphate Nanoparticle with Lipid Coating for Systemic siRNA Delivery. *J. Controlled Release* **2010**, *142*, 416−421.

(46) Yin, L. J.; Hu, S. Q.; Guo, F. [The Application of CRISPR-Cas9 Gene Editing Technology in Viral Infection Diseases]. *Yi Chuan* **2015**, *37*, 412−418.

(47) Michielse, C. B.; Hooykaas, P. J. J.; van den Hondel, C. A. M. J. J.; Ram, A. F. J. Agrobacterium-mediated Transformation as a Tool for Functional Genomics in Fungi. *Curr. Genet.* **2005**, *48*, 1−17.

(48) Arazoe, T.; Younomaru, T.; Ohsato, S.; Kimura, M.; Arie, T.; Kuwata, S. Site-specific DNA Double-strand Break Generated by I-SceI Endonuclease Enhances Ectopic Homologous Recombination in Pyricularia Oryzae. *FEMS Microbiol. Lett.* **2014**, *352*, 221−229.